IET Microwaves, Antennas & Propagation

Research Article

Optimisation of excitation tolerances for robust beamforming in linear arrays

ISSN 1751-8725
Received on 8th August 2015
Accepted on 18th September 2015
doi: 10.1049/iet-map.2015.0508
www.ietdl.org

Nicola Anselmi[1], Paolo Rocca[1], Marco Salucci[1,2], Andrea Massa[1,2] ✉

[1]*ELEDIA Research Center, Department of Information Engineering and Computer Science, University of Trento, Via Sommarive 9, 38123 Trento, Italy*
[2]*ELEDIA Offshore Lab @ Paris, Laboratoire des Signaux et Systèmes (L2S, UMR CNRS 8506), 3 rue Joliot Curie, 91192 Gif-sur-Yvette, France*
✉ *E-mail: andrea.massa@unitn.it*

Abstract: A method for robust amplitude beamforming in linear antenna arrays is presented. The admissible tolerances on the array excitations, described as real-valued intervals, are maximised regardless their nominal values, while guaranteeing that the bounds of the radiated power patterns fit a-priori defined mask constraints. A set of representative numerical results, concerned with different mask constraints as well as comparisons with state-of-the-art approaches, is reported and discussed to assess the effectiveness of the proposed approach.

1 Introduction

For many years now, the design of phased arrays is one of the most studied topic within the antenna community due to the wide number of their applications. In some key areas, like communications and radars, there is often the need of synthesising phased arrays with directive beam patterns and low secondary lobes to effectively suppress undesired signals/interferences troublesome for the system reliability [1]. Towards this purpose, a wide set of design techniques have been proposed in the literature to optimally set the array excitations [2–4], although the antenna sidelobes turn out to be significantly influenced by the accuracy in implementing these latter [5, 6]. Due to this sensitivity/dependence, robust beamforming methods for phased arrays have been introduced to yield the desired performance with an high degree of reliability through an 'over design' of the antenna layout and/or control points. For instance, a method devoted to determine the average sidelobe suppression achievable when dealing with Dolph–Chebyshev excitations [7] and tolerance errors defined as a percentage of the optimal weights has been proposed in [8]. Moreover, the computation of the array excitations that maximise the gain of the nominal array, while keeping the pattern deviations constant to random variations of the array control points around their nominal values, has been addressed in [9] by modelling the average power pattern as the superposition of the pattern generated by the nominal array plus a 'background' power level proportional to the antenna random errors. Such an approach has been successively extended in [10] to take into account the correlations among different error sources (e.g. amplitude, phase, and positions). Under the hypothesis of random deviations from the nominal weights, the direct optimisation of the performance of phased arrays has been also addressed in a probabilistic sense [11]. More recently, another robust beamforming strategy has been presented in [12] where a Monte Carlo method has been used to determine the maximum tolerance errors on the element excitations that still guarantee to fit the user-defined mask constraints for 95%. Owing to the unavoidably high computational burden, only a finite and limited number of error combinations, among the whole infinite set of possibilities, can be contemplated in such an analysis. To overcome this drawback, suitable approaches based on the interval analysis (IA) [13, 14] have been proposed in [15, 16]. Indeed, IA has been recently considered as a powerful tool in several applicative areas of engineering electromagnetics (e.g. the robust design of magnetic devices [17, 18], the radar tracking [19], and the tolerance analysis of reflector antennas [20]), thanks to its capability to naturally deal with uncertainties and tolerance errors as well as to define closed-form robust and reliable bounds by means of the arithmetic of intervals. As for robust beamforming and assuming of a-priori fixed tolerances, interval power patterns lying within mask constraints have been yielded by optimising the values of the nominal array amplitudes with a biologically inspired global optimisation algorithm in [15] and, for pencil beam patterns, through a deterministic convex minimisation procedure [16].

By taking inspiration from [12] and exploiting the features (i.e. analytic and inclusive analysis) of the IA already assessed in [15, 16], this paper is aimed at presenting a new approach, preliminary introduced in [21], to the design of robust beamforming networks of linear antenna arrays. Unlike [15, 16, 22, 23], the tolerance errors, instead of the nominal excitations, are here optimised to afford a radiation pattern fitting the user-defined masks without a-priori assumptions on the nominal array coefficients or the error distribution.

The outline of the paper is as follows. The problem is mathematically formulated in Section 2 by defining the interval power pattern as a function of the interval tolerance on the amplitude excitations. Then, the synthesis approach is described in terms of the optimisation of the excitation tolerances that guarantee the IA-computed pattern bounds satisfy user-defined constraints. In Section 3, a set of representative numerical results is reported to validate the proposed method (Section 3.1) as well as to assess its effectiveness in comparison with some state-of-the-art robust beamforming techniques (Section 3.2). Eventually, some conclusions are drawn (Section 4).

2 Mathematical formulation

Let us consider a linear antenna array of N elements, each one controlled by a transmit/receive module whose amplitude (i.e. the amplification/attenuation factor) is unknown even though belonging to the interval of real values $\boldsymbol{A}_n$ ($n = 1, \ldots, N$)

$$\boldsymbol{A}_n = \left[i_{A_n}; s_{A_n} \right] \tag{1}$$

$i_{A_n} = \inf\{\boldsymbol{A}_n\}$ and $s_{A_n} = \sup\{\boldsymbol{A}_n\}$ being the infimum (left end-point) and the supremum (right end-point) of the admissible

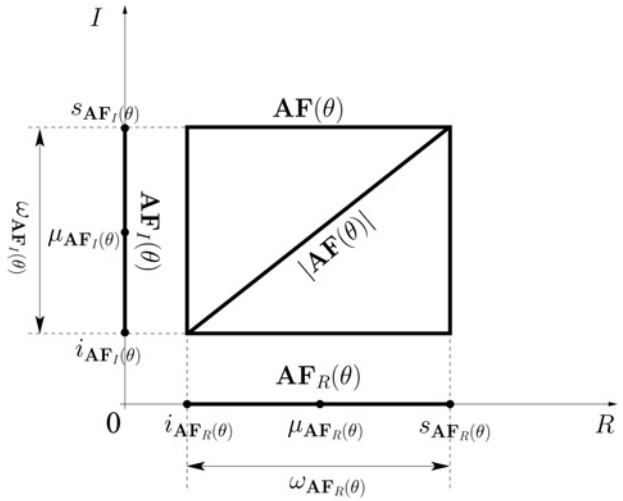

Fig. 1 *Descriptors of an interval complex value **AF(θ)***

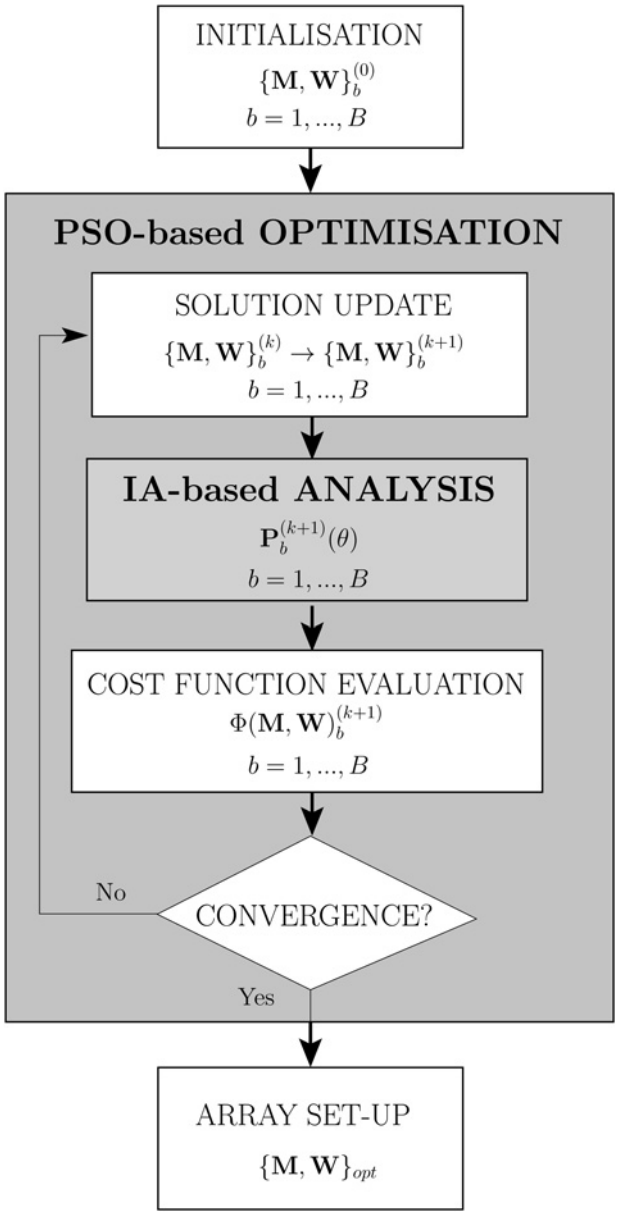

Fig. 2 *Robust beamforming method flowchart*

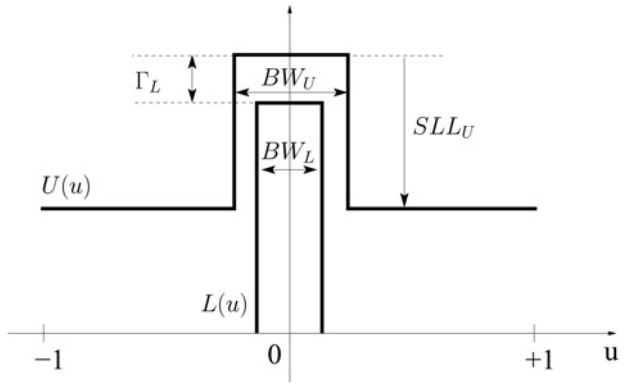

Fig. 3 *Descriptors of the power pattern mask*

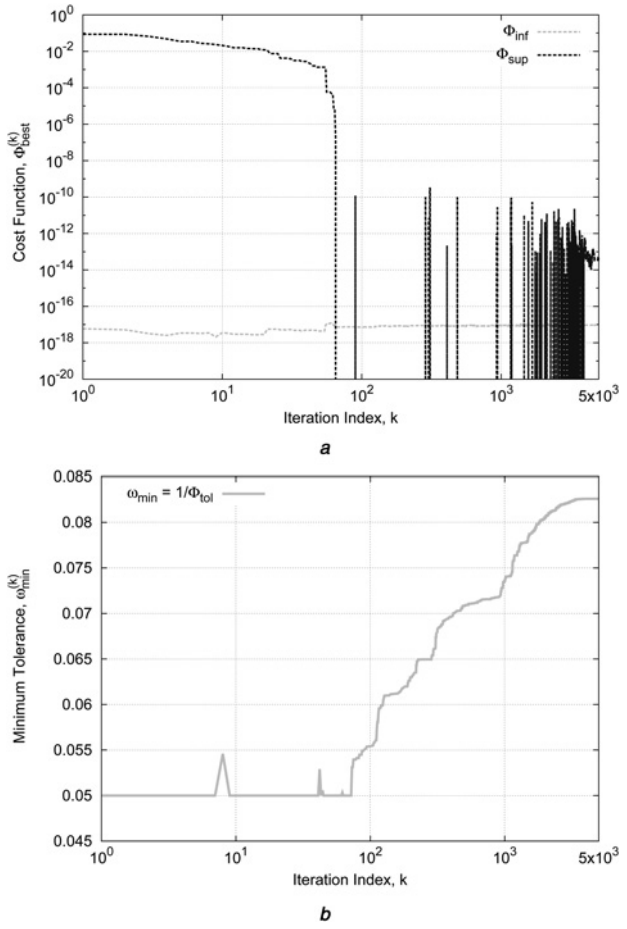

Fig. 4 *Method validation (N = 20, d = λ/2; uniform sidelobes mask: SLL_U = −20 dB, BW_U = 0.24 [u], BW_L = 0.09 [u], Γ_L = 5 dB) – behaviour of the cost function value in correspondence with the best particle of the swarm, $\{\boldsymbol{M}, \boldsymbol{W}\}_{best}^{(k)} \triangleq \min_{b=1,...,B}\{\Phi(\boldsymbol{W}, \boldsymbol{M})_b^{(k)}\}$, versus the iteration index k*

a Lower, $\Phi_{inf}(\boldsymbol{M}_{best}^{(k)}, \boldsymbol{W}_{best}^{(k)})$, and upper, $\Phi_{sup}(\boldsymbol{M}_{best}^{(k)}, \boldsymbol{W}_{best}^{(k)})$, mask misfit terms

b Optimal tolerance width, $\omega_{min}^{(k)} \triangleq 1/\Phi_{tol}^{(k)}$

amplitude values, respectively. The *width* of the *n*th interval, given by

$$\omega_{A_n} = s_{A_n} - i_{A_n}, \tag{2}$$

quantifies the tolerance range of each amplifier of the array, while the interval *mid-point*

$$\mu_{A_n} = \frac{i_{A_n} + s_{A_n}}{2} \tag{3}$$

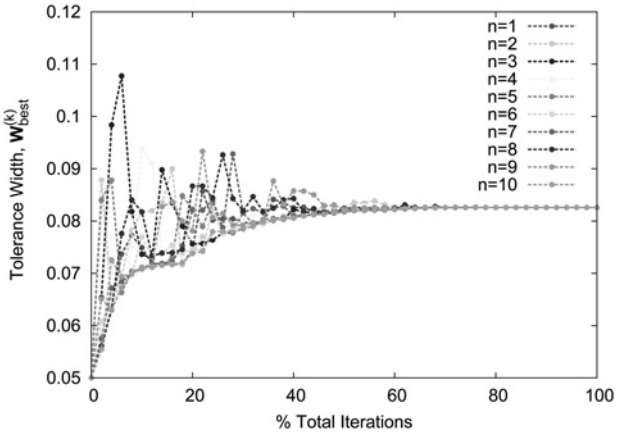

Fig. 5 *Method validation ($N = 20$, $d = \lambda/2$; uniform sidelobes mask: $SLL_U = -20$ dB, $BW_U = 0.24$ [u], $BW_L = 0.09$ [u], $\Gamma_L = 5$ dB) – widths of the interval amplitudes, $\mathbf{W}_{best}^{(k)}$, versus the iteration index k*

provides together with (2) a dual (with respect to (1)) description of the nth amplitude interval $\boldsymbol{A}_n$ since $i_{\boldsymbol{A}_n} = \mu_{\boldsymbol{A}_n} - (\omega_{\boldsymbol{A}_n}/2)$ and $s_{\boldsymbol{A}_n} = \mu_{\boldsymbol{A}_n} + (\omega_{\boldsymbol{A}_n}/2)$.

Let us now determine the analytic expression of the interval power pattern of the linear array, $\boldsymbol{P}(\theta)$, as a function of the descriptors of the interval amplitudes, namely $\mu_{\boldsymbol{A}_n}$ and $\omega_{\boldsymbol{A}_n}$ ($n = 1, \ldots, N$). The (real-valued) interval power pattern function is defined as [22] (see also Appendix)

$$\boldsymbol{P}(\theta) \triangleq |\mathbf{AF}(\theta)|^2 \tag{4}$$

$\mathbf{AF}(\theta)$ being the (complex-valued) interval array factor (Fig. 1) given by

$$\mathbf{AF}(\theta) = \sum_{n=1}^{N} \boldsymbol{A}_n \, \mathrm{e}^{\mathrm{j}[\beta(n-1)d\sin\theta + \varphi_n]} \tag{5}$$

where $\beta = 2\pi/\lambda$ is the free-space wavenumber, λ is the wavelength, d is the inter-element distance, θ is the angular rotation with respect to the boresight direction orthogonal to the array axis, and φ_n, $n = 1, \ldots, N$ is the set of error-free phase weights. The supremum and the infimum of $\boldsymbol{P}(\theta)$ are equal to [22]

$$s_{\boldsymbol{P}(\theta)} = \left(\left|\mu_{\mathbf{AF}_\mathrm{R}(\theta)}\right| + \frac{\omega_{\mathbf{AF}_\mathrm{R}(\theta)}}{2}\right)^2 + \left(\left|\mu_{\mathbf{AF}_\mathrm{I}(\theta)}\right| + \frac{\omega_{\mathbf{AF}(\theta)}}{2}\right)^2 \tag{6}$$

and (see (7)), respectively, being

$$\begin{Bmatrix} \mu_{\mathbf{AF}_\mathrm{R}(\theta)} \\ \omega_{\mathbf{AF}_\mathrm{R}(\theta)} \end{Bmatrix} = \sum_{n=1}^{N} \begin{Bmatrix} \mu_{\boldsymbol{A}_n} \\ \omega_{\boldsymbol{A}_n} \end{Bmatrix} \cos\left[\beta(n-1)d\sin\theta + \varphi_n\right] \tag{8}$$

and

$$\begin{Bmatrix} \mu_{\mathbf{AF}_\mathrm{I}(\theta)} \\ \omega_{\mathbf{AF}_\mathrm{I}(\theta)} \end{Bmatrix} = \sum_{n=1}^{N} \begin{Bmatrix} \mu_{\boldsymbol{A}_n} \\ \omega_{\boldsymbol{A}_n} \end{Bmatrix} \sin\left[\beta(n-1)d\sin\theta + \varphi_n\right]. \tag{9}$$

Let the user-defined radiation constraints be expressed as a pattern mask defined by the lower $L(\theta)$ and the upper $U(\theta)$ bounds. To determine the maximum tolerance error on the amplitude excitations still affording a

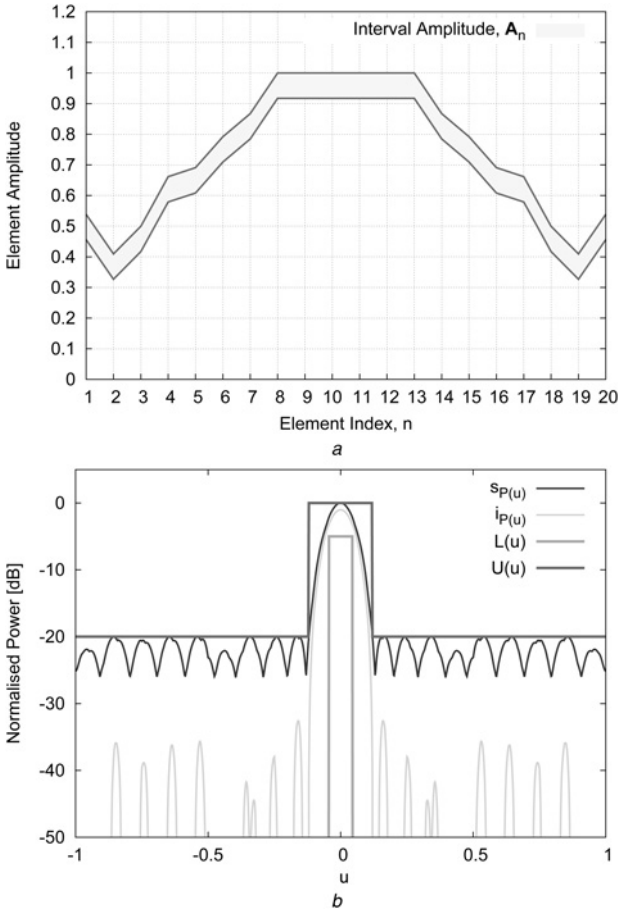

Fig. 6 *Method validation ($N = 20$, $d = \lambda/2$; uniform sidelobes mask: $SLL_U = -20$ dB, $BW_U = 0.24$ [u], $BW_L = 0.09$ [u], $\Gamma_L = 5$ dB)*

a Plots of the optimal interval amplitudes, $\boldsymbol{A}_{n,\mathrm{opt}}$, $n = 1, \ldots, N$

b Plots of the corresponding interval power pattern $\boldsymbol{P}_{\mathrm{opt}}(u)$

radiation pattern that fits the user-defined masks, the following cost function is defined

$$\Phi(\boldsymbol{W}, \boldsymbol{M}) = \alpha_{\mathrm{tol}}\Phi_{\mathrm{tol}}(\boldsymbol{W}) + \alpha_{\mathrm{inf}}\Phi_{\mathrm{inf}}(\boldsymbol{W}, \boldsymbol{M}) + \alpha_{\mathrm{sup}}\Phi_{\mathrm{sup}}(\boldsymbol{W}, \boldsymbol{M}) \tag{10}$$

and optimised by means of the particle swarm optimiser (PSO)-based procedure in Fig. 2 according to the guidelines described in [15, 24], $\boldsymbol{W} = \{\omega_{\boldsymbol{A}_n};\ n = 1, \ldots, N\}$ and $\boldsymbol{M} = \{\mu_{\boldsymbol{A}_n};\ n = 1, \ldots, N\}$ being the problem unknowns, while α_{tol}, α_{inf}, and α_{sup} are real-valued weighting coefficients. Analogously to [15], the penalty terms

$$\Phi_{\mathrm{inf}}(\boldsymbol{W}, \boldsymbol{M}) = \int_{-\pi/2}^{\pi/2} \left(L(\theta) - i_{\boldsymbol{P}(\theta)}\right) H\left\{L(\theta) - i_{\boldsymbol{P}(\theta)}\right\} \mathrm{d}\theta \tag{11}$$

and

$$\Phi_{\mathrm{sup}}(\boldsymbol{W}, \boldsymbol{M}) = \int_{-\pi/2}^{\pi/2} \left(s_{\boldsymbol{P}(\theta)} - U(\theta)\right) H\left\{s_{\boldsymbol{P}(\theta)} - U(\theta)\right\} \mathrm{d}\theta, \tag{12}$$

$H\{\circ\}$ being the Heaviside step function ($H\{\circ\} = 1$ when $\circ \geq 0$ and $H\{\circ\} = 0$, otherwise), quantify the 'mismatching' of the interval power pattern, $\boldsymbol{P}(\theta)$,

$$i_{\boldsymbol{P}(\theta)} = \begin{cases} 0 & \text{if } 0 \in \mathbf{AF}_\mathrm{R}(\theta) \text{ and } 0 \in \mathbf{AF}_\mathrm{I}(\theta) \\ \left(\left|\mu_{\mathbf{AF}_{\{\mathrm{R,I}\}}(\theta)}\right| - \dfrac{\omega_{\mathbf{AF}_{\{\mathrm{R,I}\}}(\theta)}}{2}\right)^2 & \text{if } 0 \in \mathbf{AF}_{\{\mathrm{I,R}\}}(\theta) \\ \left(\left|\mu_{\mathbf{AF}_\mathrm{R}(\theta)}\right| - \dfrac{\omega_{\mathbf{AF}_\mathrm{R}(\theta)}}{2}\right)^2 + \left(\left|\mu_{\mathbf{AF}_\mathrm{I}(\theta)}\right| - \dfrac{\omega_{\mathbf{AF}_\mathrm{I}(\theta)}}{2}\right)^2 & \text{otherwise} \end{cases}, \tag{7}$$

IET Microw. Antennas Propag., 2016, Vol. 10, Iss. 2, pp. 208–214

Table 1 Method validation ($N = 20$, $d = \lambda/2$; uniform sidelobes mask: $SLL_U = -20$ dB, $BW_U = 0.24$ [u], $BW_L = 0.09$ [u], $\Gamma_L = 5$ dB) – convergence values of $\{\boldsymbol{M}, \boldsymbol{W}\}$ and $\delta_{\boldsymbol{A}_n}$, $n = 1, \ldots, N/2$

n	1	2	3	4	5	6	7	8	9	10
$\omega_{\boldsymbol{A}_n}$					0.0826					
$\mu_{\boldsymbol{A}_n}$	0.4975	0.3682	0.4585	0.6203	0.6497	0.7507	0.8262	0.9587	0.9587	0.9587
$\delta_{\boldsymbol{A}_n}$	8.30	11.22	9.01	6.66	6.36	5.50	5.00	4.31	4.31	4.31

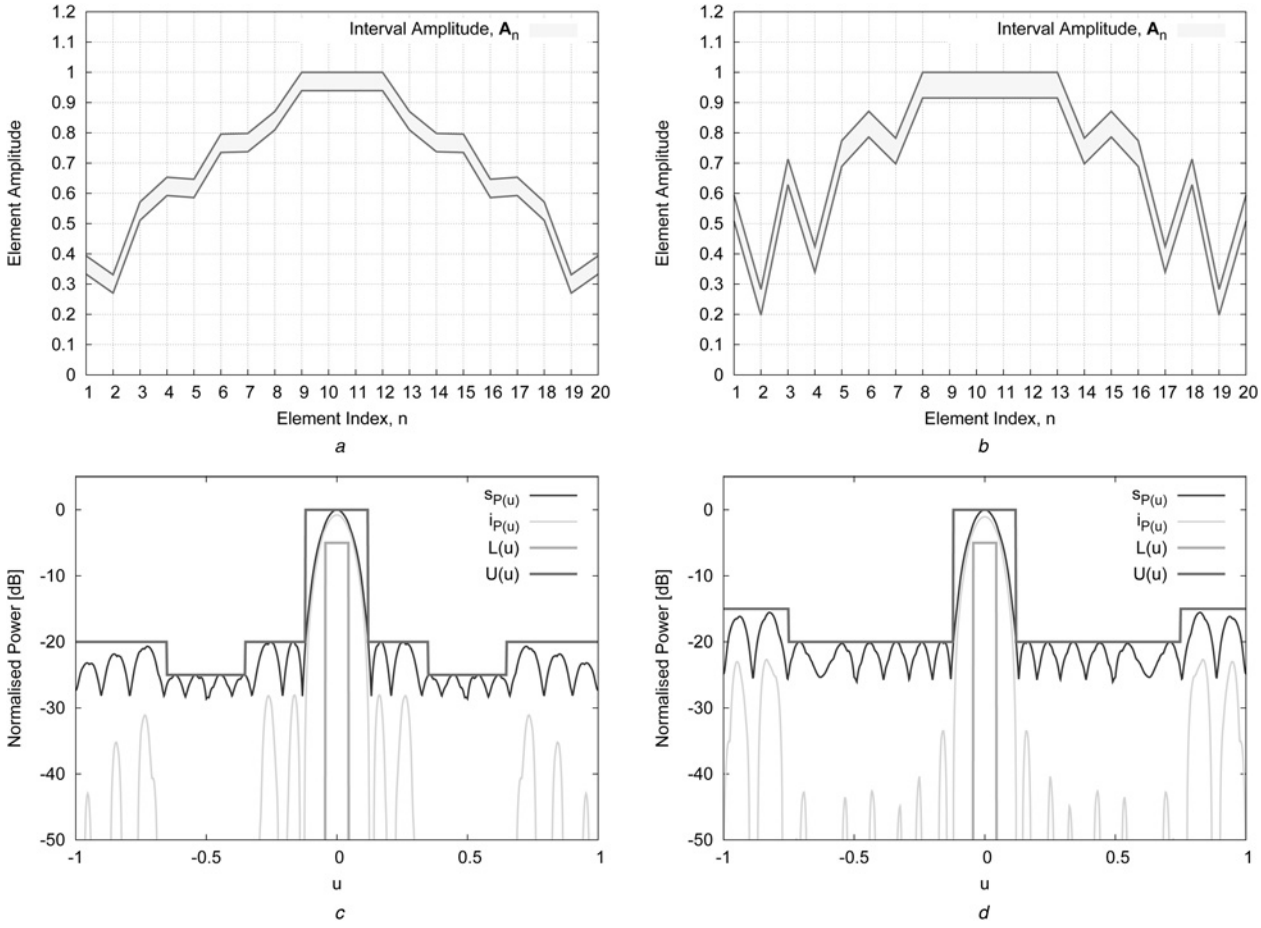

Fig. 7 *Method validation ($N = 20$, $d = \lambda/2$; reference pattern mask: $SLL_U = -20$ dB, $BW_U = 0.24$ [u], $BW_L = 0.09$ [u], $\Gamma_L = 5$ dB)*

a, b Plots of the optimal interval amplitudes, $\boldsymbol{A}_{n,\text{opt}}$, $n = 1, \ldots, N$

c, d Plots of the corresponding interval power pattern $\boldsymbol{P}_{\text{opt}}(u)$ when setting a sidelobe depression of 5 dB within $u = [\pm 0.35: \pm 0.65]$ (Figs. 7*a* and *c*) and a sidelobe increment of 8 dB at $u = [\pm 0.80: \pm 1.00]$ (Figs. 7*b* and *d*) within the reference pattern mask

with the mask constraints, while the remaining term in (10)

$$\Phi_{\text{tol}}(\boldsymbol{W}) = \frac{1}{\omega_{\min}} \tag{13}$$

being $\omega_{\min} \triangleq \min_{n=1,\ldots,N} \{\omega_{\boldsymbol{A}_n}\}$, forces the maximisation of the admissible amplitude tolerance to improve as much as possible the robustness of the beamforming configuration.

It is worth observing that because of (11) and (12), the cost function not only depends on $\boldsymbol{W}$, but also $\boldsymbol{M}$ since the interval amplitudes $\boldsymbol{A}_n$, $n = 1, \ldots, N$, need to be determined to compute the interval power pattern bounds through (6) and (7). However, (13) is only function of $\boldsymbol{W}$ and it does not depend on the nominal excitation values or interval mid-points.

3 Numerical results

In this section, the robust beamforming method is first assessed by means of representative results concerned with the design of linear

Table 2 Method validation ($N = 20$, $d = \lambda/2$; non-uniform sidelobes masks) – convergence values of $\{\boldsymbol{M}, \boldsymbol{W}\}$ and $\delta_{\boldsymbol{A}_n}$, $n = 1, \ldots, N/2$

n	1	2	3	4	5	6	7	8	9	10
					Sidelobe depression					
$\omega_{\boldsymbol{A}_n}$					0.0607					
$\mu_{\boldsymbol{A}_n}$	0.3630	0.3010	0.5414	0.6228	0.6163	0.7655	0.7679	0.8401	0.9697	0.9697
$\delta_{\boldsymbol{A}_n}$	8.35	10.09	5.60	4.87	4.92	3.96	3.95	3.61	3.13	3.13
					End-fire sidelobe increment					
$\omega_{\boldsymbol{A}_n}$					0.0849					
$\mu_{\boldsymbol{A}_n}$	0.5510	0.2399	0.6711	0.3820	0.7314	0.8286	0.7340	0.9576	0.9576	0.9576
$\delta_{\boldsymbol{A}_n}$	7.7	17.69	6.32	11.11	5.8	5.12	5.74	4.43	4.43	4.43

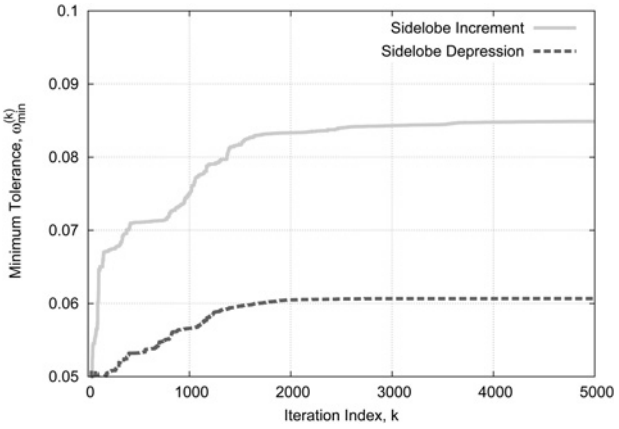

Fig. 8 *Method validation ($N = 20$, $d = \lambda/2$; reference pattern mask: $SLL_U = -20$ dB, $BW_U = 0.24$ [u], $BW_L = 0.09$ [u], $\Gamma_L = 5$ dB) – behaviour of $\omega_{min}^{(k)}$ versus the iteration index k in case of non-uniform power pattern masks*

arrays with secondary lobes having uniform and non-uniform behaviours. Successively, a comparative assessment is carried out by considering benchmark examples from the literature, namely [15, 16]. In all examples, the optimisation of the two sets of unknown parameters, $\boldsymbol{W} = \{\omega_{A_n}; n = 1, \ldots, N\}$ and $\boldsymbol{M} = \{\mu_{A_n}; n = 1, \ldots, N\}$, is addressed through the PSO with the following calibration setup [24]: $B = N$ (B being the swarm dimension), $w = 0.4$ (w being the inertial weight), $C_1 = C_2 = 2.0$ (C_1 and C_2 being the cognitive and the social acceleration coefficients, respectively), and $K = 5 \times 10^3$ (K being the maximum number of iterations). All simulations have been performed on a standard laptop PC at 2.4 GHz CPU with 2 GB of RAM by running a non-optimised software. As for the weighting coefficients in (10), they have been chosen equal to $\alpha_{inf} = \alpha_{sup} = 1$ and $\alpha_{tol} = 10^{-5}$. This latter value has been selected since the threshold $\Phi = 10^{-5}$ has been found in [15] to be satisfactory to yield an interval power pattern fitting the mask constraints, thus it is expected that the optimisation acts on the tolerance parameter, ω_{min}, mainly after the pattern bounds satisfaction.

3.1 Method validation

Let us consider a linear array of $N = 20$ $d = \lambda/2$-spaced elements. The power pattern mask has been chosen as shown in Fig. 3 by setting $SLL_U = -20$ dB, $BW_U = 0.24[u]$, $BW_L = 0.09[u]$, and $\Gamma_L = 5$ dB ($u = \sin\theta$). Due to the symmetric constraints and the main lobe directed along boresight, $\theta_0 = 0^\circ$ ($u_0 = 0$), the phase weights turned out to be $\varphi_n = 0$, $n = 1, \ldots, N$ as (5). Under these hypothesis, only the amplitudes of half elements of the array ($n = 1, \ldots, N/2$) have been optimised. Without loss of generality, the admissible values of these coefficients have been assumed normalised and the lower threshold of the minimum tolerance width has been set to $\omega_{lb} = 0.05$ to keep (13) finite.

Fig. 4 shows the behaviour of the cost function during the optimisation process. The values of the cost function terms in correspondence with the global best solution of the swarm, namely

$$\{\boldsymbol{M}, \boldsymbol{W}\}_{\text{best}}^{(k)} \triangleq \arg \min_{b=1,\ldots,B} \left\{\Phi(\boldsymbol{W}, \boldsymbol{M})_b^{(k)}\right\}, \tag{14}$$

are given versus the iteration index, k, until convergence (i.e. $k = K$) is reached after 14 min. More specifically, the misfits with the lower

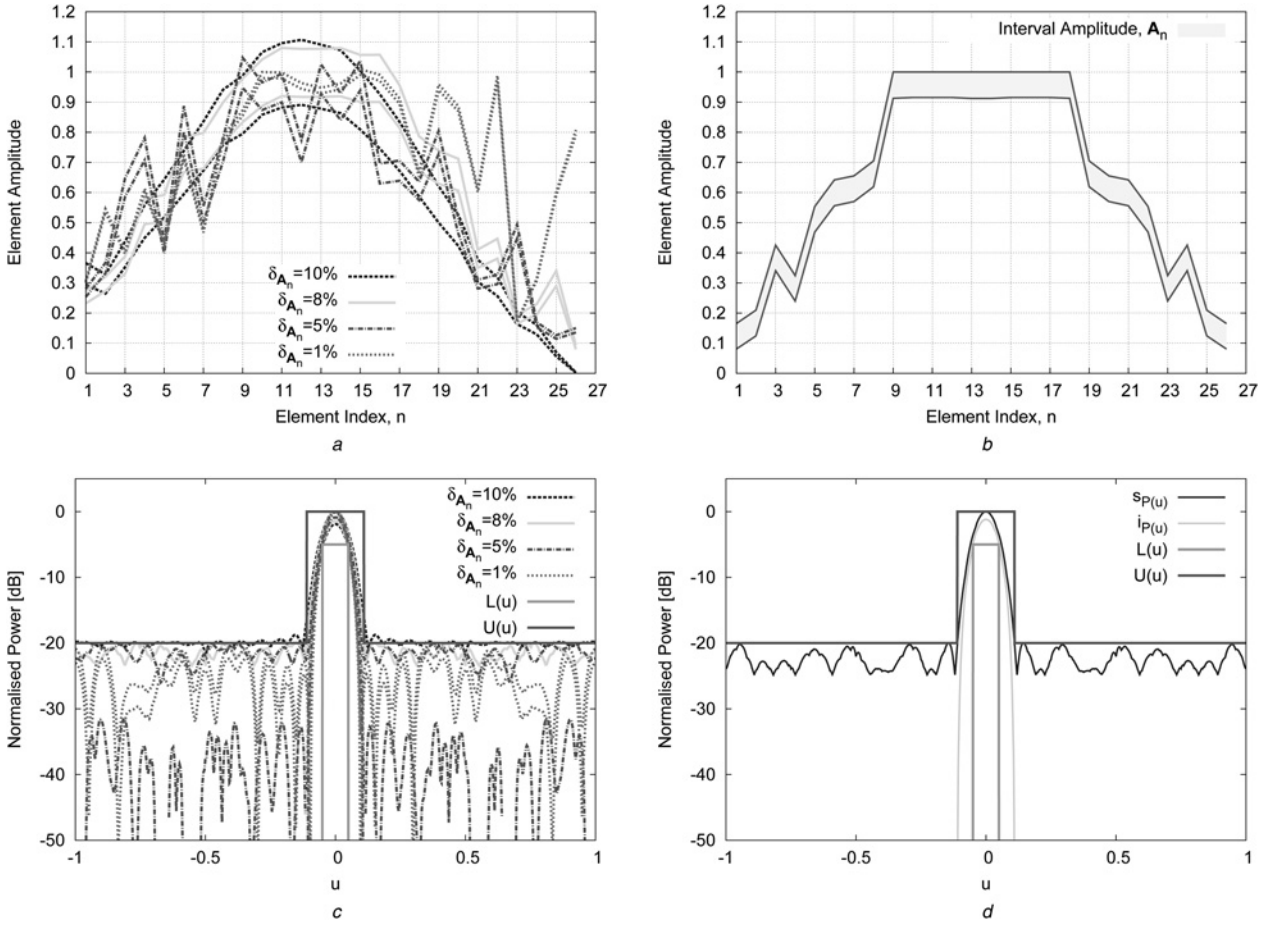

Fig. 9 *Comparative assessment (benchmark case [15]: $N = 26$, $d = \lambda/2$; uniform sidelobes mask: $SLL_U = -20$ dB, $BW_U = 0.22$ [u], $BW_L = 0.10$ [u], $\Gamma_L = 5$ dB)*

a, b Plots of the optimal interval amplitudes, $\boldsymbol{A}_{n,\text{opt}}$, $n = 1, \ldots, N$

c, d Plots of the corresponding interval power patterns, $\boldsymbol{P}_{\text{opt}}(u)$, synthesised with the method in [15] (Figs. 9*a* and *c*) setting $\delta_{\text{avg}} = \{1, 5, 8, 10\}\%$ and the proposed approach (Figs. 9*b* and *d*)

IET Microw. Antennas Propag., 2016, Vol. 10, Iss. 2, pp. 208–214

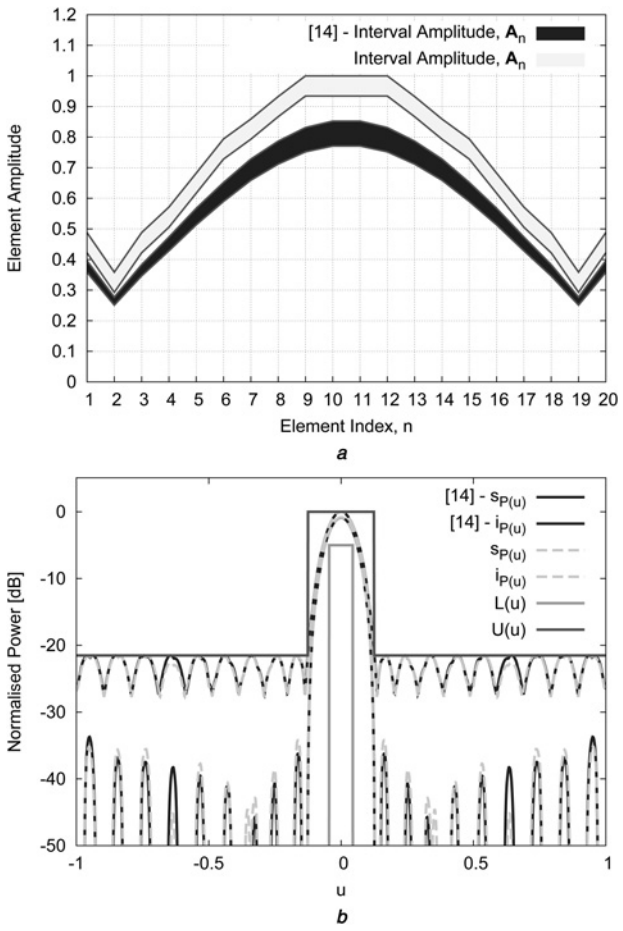

Fig. 10 *Comparative assessment (benchmark case [16]: $N = 20$, $d = \lambda/2$; $SLL_U = -21.5$ dB, $BW_U = 0.25$ [u], $BW_L = 0.10$ [u], $\Gamma_L = 5$ dB)*

a Plots of the optimal interval amplitudes, $\boldsymbol{A}_{n,\text{opt}}$, $n = 1, \ldots, N$

b Plots of the corresponding interval power patterns, $\boldsymbol{P}_{\text{opt}}(u)$, synthesised with the method in [16] setting $\delta_{\text{avg}} = 5\%$ and the proposed approach

(11) and the upper (12) mask constraints are reported in Fig. 4*a*, while the tolerance width (i.e. the inverse of (13)) is displayed in Fig. 4*b*. As it can be observed (Fig. 4*b*), the minimum tolerance width, $\omega_{\text{min}}^{(k)} = \min_{n=1,\ldots,N}\left\{\boldsymbol{W}_{\text{best}}^{(k)}\right\}$, $k = 1, \ldots, K$, increases after the first iterations throughout the whole optimisation process until $\omega_{\text{opt}} = \omega_{\text{min}}^{(K)} = 8.26 \times 10^{-2}$ that is an increment of almost 65% with respect to its initial value, ω_{lb}.

Another interesting outcome is outlined by the plots in Fig. 5 where the entries of the vector $\boldsymbol{W}_{\text{best}}^{(k)}$ are shown at various steps of the optimisation process. At the beginning, the tolerance errors on the array elements are different. In some cases, there are elements having tolerances twice the minimum value, $\omega_{\text{min}}^{(k)}$. Throughout the PSO optimisation, $\omega_{\text{min}}^{(k)}$ increases and the differences among the tolerances minimise. Towards the convergence, all array elements have almost the same tolerance value.

Fig. 6*a* and Table 1 give the values $\{\boldsymbol{M}, \boldsymbol{W}\}_{\text{opt}}$ defining the optimal interval amplitude coefficients $\boldsymbol{A}_{\text{opt}}$, while the corresponding interval power pattern, $\boldsymbol{P}_{\text{opt}}(u)$ (i.e. its upper and lower bounds), is shown in Fig. 6*b*. As expected, the mask requirements are fully satisfied (Fig. 6*b*). To give a quantitative indication on the robustness of the optimised beamforming networks, the following index has been computed:

$$\delta_{A_n} = \left(\frac{\omega_{A_n}}{2} \times \frac{1}{\mu_{A_n}}\right) \times 100, \quad n = 1, \ldots, N \tag{15}$$

for each element of the array (Table 1) along with its average, $\delta_{\text{avg}} = 1/N \sum_{n=1}^{N} \delta_{A_n}$. Having in mind that the lowest robustness corresponds to $\delta_{\text{avg}} = 0.0$, we have in our case $\delta_{\text{avg}} = 6.50$.

The second example deals with masks having non-uniform upper bounds, $U(u)$, as shown in Figs. 7*c* and *d*. With reference to the mask of the previous example, a sidelobe depression of 5 dB has been set within the angular range $u = [\pm 0.35 : \pm 0.65]$ in the first test case, while the second one considered a sidelobe increment of 8 dB close to the end-fire direction at $u = [\pm 0.80 : \pm 1.00]$. After 12 min, the PSO-optimised amplitudes turned out to be as shown in Figs. 7*a* and *b* with values reported in Table 2. As it can be observed, the upper bounds $s_{P(\theta)}$ of the synthesised interval power patterns follow the staircase behaviour of $U(u)$ with sidelobe depressions (Fig. 7*c*) or an increase of the sidelobe level close to end-fire (Fig. 7*d*), while always $s_{P(\theta)} > i_{P(\theta)} \geq L(u)$, $\forall [u \in -1{:}1]$. Concerning the minimum width $\omega_{\text{min}}^{(k)}$ shown in Fig. 8, it increases during the optimisation whatever the test case at hand, even though the value at the convergence turns out to be higher for Fig. 7*b* than that in correspondence with Fig. 7*a*, due to the lighter sidelobe requirements (Fig. 7*d*). Likewise the previous example, all elements of the array present at convergence an equal tolerance error that amounts to $\omega_{\text{opt}} = 6.07 \times 10^{-2}$ (Fig. 7*a*) and $\omega_{\text{opt}} = 8.49 \times 10^{-2}$ (Fig. 7*b*), respectively, with an enhanced robustness of almost 21 and 70%, respectively, with respect to the tolerance initialisation. Quantitatively, the average tolerances amount to $\delta_{\text{avg}} = 5.16$ and $\delta_{\text{avg}} = 7.28$ for the beamforming configurations in Figs. 7*a* and *b*, respectively. By observing the optimised distributions of the interval amplitudes, there is a smooth transition between adjacent elements in Fig. 7*a*, while sharper variations arise in Fig. 7*b*.

3.2 Comparative assessment

For comparison purposes, let us refer to the IA-based approaches presented in [15, 16]. Concerning the latter, it is worthwhile remembering that the values of the nominal excitations have been optimised under the hypothesis of fixed tolerance errors, thus the resulting value of δ_{A_n}, computed as in (15) by substituting μ_{A_n} with the nominal value, turns out to be equal for all array elements and a-priori fixed to $\delta_{A_n} = \delta_{\text{avg}}$. Differently, the proposed approach is aimed at maximising the amplitude tolerance widths, ω_{A_n}, $n = 1, \ldots, N$, and therefore the value of δ_{avg}, to look for the most robust beamforming setup fitting the pattern masks.

The first comparative benchmark example deals with mask constraints $L(u)$ and $U(u)$ set as in [15] (i.e. $SLL_U = -20$ dB, $BW_U = 0.22$ [u], $BW_L = 0.10$ [u], and $\Gamma_L = 5$ dB) and a half-wavelength array of $N = 26$ elements. In [15], four different simulations have been run by a-priori setting $\delta_{A_n} = \delta_{\text{avg}} = \{1, 5, 8, 10\}$, to yield the interval amplitude excitations and the corresponding interval power patterns shown in Figs. 9*a* and *c*, respectively. From the pattern plots, one can notice that the solution optimised when $\delta_{\text{avg}} = 1$ fully lies within the lower and upper masks, but its bounds are far from the mask limits. This means that larger excitation uncertainties can be admitted. Indeed, the interval pattern for tolerances as $\delta_{\text{avg}} = 5$ still works, while larger deviations from the nominal value (starting from $\delta_{\text{avg}} = 8$ and more significantly when $\delta_{\text{avg}} = 10$) turn out to be unsatisfactory. On the contrary, the proposed approach allows one to yield the solution in Figs. 9*b* and *d* having an average tolerance of $\delta_{\text{avg}} = 10.8$ ($\omega_{\text{opt}} = 8.54 \times 10^{-2}$).

Let us now consider the method in [16] where the robust beamforming synthesis of pencil beams has been recast as the maximisation of the peak value of $i_{P(\theta)}$ subject to the upper bound $U(u)$ on the secondary lobes of $s_{P(\theta)}$. Owing to the convexity of the problem, the unique global optimum of the cost function at hand has been computed with a deterministic method [16], but analogously to [15], a key limitation for some engineering applications is still the a-priori assumption on the value of δ_{avg}. For a fair comparison, the new approach under analysis has been run on the same test in [16] with $N = 20$, $d = \lambda/2$, and $\delta_{\text{avg}} = 5$, by defining a pattern mask including the interval power pattern synthesised with the convex optimisation [16] (i.e. $SLL_U = -21.5$ dB, $BW_U = 0.25$ [u], $BW_L = 0.10$ [u], and $\Gamma_L = 5$ dB). At the PSO

convergence, the minimum tolerance error was equal to $\omega_{opt} = 6.57 \times 10^{-2}$ and the robustness of the beamforming architecture has been increased to $\delta_{avg} = 5.44$. For completeness, the arising interval amplitudes, $\boldsymbol{A}_n$, $n = 1, \ldots, N$, and the corresponding interval pattern, $\boldsymbol{P}(u)$, are shown in Figs. 10*a* and *b*, respectively, along with the results in [16].

4 Conclusions

The design of robust linear arrays radiating reliable power patterns regardless the uncertainties on the amplitude coefficients of the beamforming network has been addressed. The amplitude tolerance has been maximised without a-priori hypothesis/assumptions on the error distribution or reference/nominal excitations, while forcing the bounds of the arising power pattern to satisfy user-defined mask-power constraints. Towards this end, a hybrid approach integrating the PSO for optimising the amplitude tolerances and the IA-based analysis for analytically defining the inclusive interval bounds of the power pattern has been presented. The numerical assessment has shown that the proposed approach provides a powerful tool for designing robust beamforming weights and effectively compares with the state-of-the-art literature, thanks to its capability to directly encompass the maximisation of the admissible tolerance error in the optimisation step.

Future advances, out-of-the scope of this paper, are expected in planar array synthesis and optimisation of other descriptors of the array control points (e.g. element phases or positions).

5 Acknowledgments

This work was benefited from the networking activities carried out within the SIRENA project (2014–2017) funded by DIGITEO (France) under the 'Call for Chairs 2014'.

6 References

1 Mailloux, R.J.: 'Phased array antenna handbook' (Artech House, 2005)
2 Van Trees, H.L.: 'Optimum array processing (part IV)' (Wiley & Sons, 2002)
3 Elliott, R.S.: 'Antenna theory and design' (Wiley & Sons, 2003)
4 Haupt, R.L.: 'Antenna arrays – a computation approach' (Wiley & Sons, 2010)
5 Ruze, J.: 'The effect of aperture errors on the antenna radiation pattern', *Nuovo Cimento Suppl.*, 1952, **9**, pp. 364–380
6 Elliott, R.E.: 'Mechanical and electrical tolerances for two-dimensional scanning antenna arrays', *Trans. IRE Antennas Propag.*, 1958, **6**, pp. 114–120
7 Dolph, C.L.: 'A current distribution for broadside arrays which optimizes the relationship between beam width and side-lobe level', *Proc. IRE*, 1946, **34**, pp. 335–348
8 Ashmead, D.: 'Optimum design of linear arrays in the presence of random errors', *Trans. IRE Antennas Propag.*, 1952, **4**, pp. 81–92
9 Gilbert, E.N., Morgan, S.P.: 'Optimum design of directive antenna arrays subject to random variations', *Bell Syst. Tech. J.*, 1995, **34**, p. 637463
10 Tseng, F.I., Cheng, D.K.: 'Gain optimization for antenna arrays with random errors in design parameters', *IEEE Proc.*, 1966, **54**, pp. 1455–1456
11 Richards, W.F., Lo, Y.T.: 'Antenna pattern synthesis based on optimization in probabilistic sense', *IEEE Trans. Antennas Propag.*, 1975, **23**, pp. 165–172
12 Lee, J., Lee, Y., Kim, H.: 'Decision of error tolerance in array element by the Monte Carlo method', *IEEE Trans. Antennas Propag.*, 2005, **53**, pp. 1325–1331
13 Boche, R.: 'Complex interval arithmetic with some applications'. Technical Report, Lockheed Missiles & Space Company, Sunnyvale, California, 1966, pp. 1–33
14 Moore, R.E., Kearfott, R.B., Cloud, M.J.: 'Introduction to interval analysis' (SIAM, 2009)
15 Manica, L., Anselmi, N., Rocca, P., *et al.*: 'Robust mask-constrained linear array synthesis through an interval-based particle swarm optimization', *IET Microw. Antennas Propag.*, 2013, **7**, pp. 976–984
16 Rocca, P., Anselmi, N., Massa, A.: 'Optimal synthesis of robust beamformer weights exploiting interval analysis and convex optimization', *IEEE Trans. Antennas Propag.*, 2014, **62**, pp. 3603–3612
17 Saxena, G., Lowther, D.A.: 'The use of interval mathematics in electromagnetic design', *IEEE Trans. Mag.*, 2001, **37**, pp. 3588–3591
18 Egiziano, L., Lamberti, P., Spagnuolo, G., *et al.*: 'Robust design of electromagnetic systems based on interval Taylor extension applied to a multiquadric performance function', *IEEE Trans. Mag.*, 2008, **44**, pp. 1134–1137
19 Soares, G.L., Arnold-Bos, A., Jaulin, L., *et al.*: 'An interval-based target tracking approach for range-only multistatic radar', *IEEE Trans. Mag.*, 2008, **44**, pp. 1350–1353
20 Rocca, P., Anselmi, N., Massa, A.: 'Interval arithmetic for pattern tolerance analysis of parabolic reflectors', *IEEE Trans. Antennas Propag.*, 2014, **62**, pp. 4952–4960
21 Anselmi, N., Rocca, P., Massa, A., *et al.*: 'Synthesis of robust beamforming weights in linear antenna arrays'. Proc. of 2014 IEEE Antenna Conf. on Antenna Measurements and Applications (IEEE CAMA 2014), Antibes Juan-les-Pins, France, 16–19 November 2014, pp. 1–3
22 Anselmi, N., Manica, L., Rocca, P., *et al.*: 'Tolerance analysis of antenna arrays through interval arithmetic', *IEEE Trans. Antennas Propag.*, 2013, **61**, pp. 5496–5507
23 Rocca, P., Manica, L., Anselmi, N., *et al.*: 'Analysis of the pattern tolerances in linear arrays with arbitrary amplitude errors', *IEEE Antennas Wirel. Propag. Lett.*, 2013, **12**, pp. 639–642
24 Rocca, P., Benedetti, M., Donelli, D., *et al.*: 'Evolutionary optimization as applied to inverse scattering problems', *Inverse Probl.*, 2009, **25**, pp. 1–41

7 Appendix: absolute value of a complex interval

Given the complex interval $\mathbf{AF}(\theta) = \mathbf{AF}_R(\theta) + j\mathbf{AF}_I(\theta)$, $\mathbf{AF}_R(\theta)$ and $\mathbf{AF}_I(\theta)$ being its real-valued interval real and imaginary parts, the corresponding absolute value is defined as

$$\left|\mathbf{AF}(\theta)\right| = \sqrt{\mathbf{AF}_R^2(\theta) + \mathbf{AF}_I^2(\theta)} \tag{16}$$

where the square of $\boldsymbol{X} \triangleq \mathbf{AF}_{\langle R,I\rangle}(\theta)$ is given as

$$\boldsymbol{X}^2 = \begin{cases} \left[\left(\min\{i_X, s_X\}\right)^2; \left(\max\{i_X, s_X\}\right)^2\right] & \text{if } 0 \notin \boldsymbol{X} \\ \left[0; \left(\max\{i_X, s_X\}\right)^2\right] & \text{if } 0 \in \boldsymbol{X} \end{cases} \tag{17}$$

and the square root of $\boldsymbol{Y} \triangleq \left(\mathbf{AF}_R^2(\theta) + \mathbf{AF}_I^2(\theta)\right)$ is

$$\sqrt{\boldsymbol{Y}} = \left[\sqrt{i_Y}; \sqrt{s_Y}\right] \tag{18}$$

with $i_Y \geq 0$.